AGU PUBLICATIONS

JGR

Journal of Geophysical Research: Atmospheres

RESEARCH ARTICLE
10.1002/2016JD026250

Key Points:
- We propose a hybrid method for estimating surface downward longwave radiation from MODIS
- The bias and RMSE of the proposed method are 0.0597 W/m^2 and 21.008 W/m^2
- The accuracy of our method is superior to that of other studies reported in the literature

Correspondence to:
J. Cheng,
brucechan2003@126.com

Citation:
Cheng, J., S. Liang, W. Wang, and Y. Guo (2017), An efficient hybrid method for estimating clear-sky surface downward longwave radiation from MODIS data, *J. Geophys. Res. Atmos.*, *122*, 2616–2630, doi:10.1002/2016JD026250.

Received 16 NOV 2016
Accepted 16 FEB 2017
Accepted article online 19 FEB 2017
Published online 3 MAR 2017

An efficient hybrid method for estimating clear-sky surface downward longwave radiation from MODIS data

Jie Cheng[1], Shunlin Liang[1,2], Wenhui Wang[3], and Yamin Guo[1]

[1]State Key Laboratory of Remote Sensing Science, Faculty of Geographical Science, Beijing Normal University, Beijing, China, [2]Department of Geographical Science, University of Maryland, College Park, Maryland, USA, [3]Earth Resource Technology, Inc., NCWCP, College Park, Maryland, USA

Abstract This paper proposes an efficient hybrid method for estimating 1 km instantaneous clear-sky surface downward longwave radiation (LWDN) from Moderate Resolution Imaging Spectroradiometer (MODIS) thermal infrared observations and the MODIS near-infrared column water vapor (CWV) data product. The LWDN was formulated as a nonlinear function of surface upwelling longwave radiation estimated from the MODIS top-of-atmosphere (TOA) radiance of channels 29, 31, and 32, as well as CWV and the MODIS TOA radiance of channel 29. Ground measurements collected at 62 globally distributed sites from six networks were used to develop and validate the proposed hybrid method. The validation results showed that the bias and root-mean-square error (RMSE) were 0.0597 W/m^2 and 21.008 W/m^2. These results demonstrate that the performance of our method is superior to that of other studies reported in the literature. The drawback of our method is that LWDN is overestimated over high-elevation areas with extremely low CWV ($<$0.5 g/cm^2) and underestimated over regions with tropical climates that have extremely high CWV. A power function relating LWDN to CWV was derived and used as a complementary method to address these circumstances. The overestimation was overcome, and the bias and RMSE decreased from 9.407 W/m^2 and 23.919 W/m^2 to $-$0.924 W/m^2 and 19.895 W/m^2. The underestimation was also alleviated.

1. Introduction

The surface energy budget plays an important role in controlling Earth's hydrological, ecological, and biogeochemical processes [*Liang et al*., 2010b; *Wild et al*., 2014; *Yang et al*., 2010]. Surface downward longwave radiation (LWDN, 4–100 μm) is one of the four components of surface net radiation, which is the key driving force for evapotranspiration.

LWDN is emitted by the atmosphere itself, mainly by H_2O, CO_2, and O_3 molecules as well as by aerosols, water droplets, and ice crystals in clouds and fog. LWDN is dominated by the radiation from a shallow layer close to the surface of the Earth [*Ellingson*, 1995; *Gupta et al*., 2010; *Schmetz*, 1989; *Wang and Dickinson*, 2013]. The atmosphere above 500 m from the surface accounts for only 16–20% of the total LWDN, and the contribution of the lowest 10 m of the atmosphere accounts for 32–36% of the LWDN [*Schmetz*, 1989]. The clear-sky LWDN depends on the vertical profiles of atmospheric temperature, moisture, and the abundances of other gases [*Ellingson*, 1995; *Lee*, 1993; *Lee and Ellingson*, 2002]. Previous studies have indicated that the profiles of atmospheric temperature and moisture are the most important parameters for estimating clear-sky LWDN. It is sufficient to use the climatological CO_2 and O_3 mass mixing ratios because variations in the mixing ratios of these two gases have small effects on LWDN. A 50% change in the mixing ratios of these two species modifies LWDN by only 1 W m^{-2} [*Smith and Wolfe*, 1983]. The weighting function of LWDN is peaked close to the surface, and correctly accounting for air temperature close to the surface is critical for realistic LWDN estimates [*Gupta et al*., 2010]. Thus, air temperature and/or water vapor pressure at screening level are always used to estimate clear-sky LWDN in parameterizations [*Idso*, 1968; *Swinbank*, 1963; *Wang and Dickinson*, 2013].

Satellite remote sensing is the only means of estimating LWDN at regional and global scales. It can provide products with various spatial and temporal resolutions at relatively low cost. During the past several decades, significant efforts have been devoted to estimating LWDN [*Diak et al*., 2005; *Ellingson*, 1995; *Liang et al*., 2010a; *Schmetz*, 1989; *Wang and Dickinson*, 2013]. The methods that have been developed can be divided into three categories: profile-based (physical) methods, parameterizations, and hybrid methods. 1. Profile-based methods [*Dubayah*, 1995] calculate LWDN using radiative transfer models and satellite-derived atmospheric parameters, including atmospheric profiles and cloud parameters. The advantage of profile-based methods is

that they are physics based. One of their major disadvantages is that errors in the input parameters affect the accuracy of the derived LWDN. Moreover, atmospheric parameters are expensive to obtain, and they are not always available. 2. Parameterizations [*Brutsaert*, 1975; *Carmona et al*., 2014; *Prata*, 1996] estimate LWDN using screen-level (approximately 2 m above the surface) air temperature and/or moisture measurements. Parameterizations are usually site specific, and the coefficients used in parameterizations may vary significantly by site [*Brunt*, 1932; *Iziomon et al*., 2003; *Monteith and Szeicz*, 1961; *Swinbank*, 1963]. For example, different coefficients have been reported for the widely used clear-sky atmospheric emissivity model developed by *Brunt* [1932], with variability as large as 32% [*Iziomon et al*., 2003; *Monteith and Szeicz*, 1961; *Swinbank*, 1963]. It is hard to acquire accurate air temperature and moisture from remote sensing, and the accuracy of meteorological parameter-based models depends on the suitability of the model to the local atmospheric conditions and the data used for model calibration. 3. Hybrid methods [*Lee and Ellingson*, 2002; *Tang and Li*, 2008; *Wang and Liang*, 2009] typically begin by simulating LWDN and top-of-atmosphere (TOA) spectral radiance for a particular sensor using a radiative transfer model and a large number of representative atmospheric profiles. Empirical relationships between LWDN and the TOA radiance or the brightness temperature are then established using statistical analysis or machine learning techniques. The physics that govern LWDN are embedded in the radiative transfer simulation process.

Hybrid methods do not require real-time atmospheric parameters and have an explicit physical basis; they can also achieve acceptable accuracy at the same time. Thus, estimating LWDN from remote sensing data, especially data from the Moderate Resolution Imaging Spectroradiometer (MODIS), is gaining in popularity. MODIS provides the opportunity to estimate the surface longwave radiation budget at a spatial resolution of 1 km, which is highly important for high spatial resolution (down to 1 km) numerical weather prediction models and land surface models. For example, Tang and Li developed a linear model for estimating clear-sky LWDN globally using MODIS TOA radiance. The bias and root-mean-square error (RMSE) of their model at six sites in the Surface Radiation Budget Network (SURFRAD) network are 20.3 W/m^2 and 30.1 W/m^2 [*Tang and Li*, 2008]. Wang and Liang derived new linear and nonlinear models for estimating LWDN over the North American continent; the RMSE of their model is approximately 6–19 W/m^2 smaller than that of Tang and Li's linear model at the five SURFRAD validation sites that the two studies have in common [*Wang and Liang*, 2009]. Wang and Liang also developed hybrid methods for estimating LWDN using data from GOES Sounders and GOES-R ABI, achieving comparable accuracy [*Wang and Liang*, 2010]. Wang *et al*. proposed an artificial neural network (ANN)-based hybrid method for estimating surface longwave radiative flux components over the midlatitude regions [*Wang et al*., 2013]. They concluded that incorporating atmospheric temperature and water vapor profiles as inputs to the ANN can improve the accuracy of LWDN retrieval. The bias and RMSE of the validation over seven sites in the SURFRAD network are −8.8 W/m^2 and 20.1 W/m^2. Clearly, hybrid methods achieve better results in estimating regional LWDN from MODIS data. However, an efficient hybrid method that operates at global scale is currently unavailable.

The meteorological, hydrological, and agricultural research communities require an accuracy of 5–10 W/m^2 for LWDN retrieved from satellite data at a 25–100 km spatial resolution and 3 h daily temporal resolution [*CEOS and WMO*, 2000]. The acceptable accuracy for satellite-derived instantaneous LWDN is 20 W/m^2 [*Gupta et al*., 2004].The purpose of this paper is to develop an efficient hybrid method for estimating high spatial resolution instantaneous clear-sky LWDN from MODIS data. The remainder of the paper is organized as follows: the satellite data and ground measurements used, as well as the principles underlying the proposed hybrid method, are introduced in section 2. The results of the LWDN estimation are provided in section 3. A full error analysis and validation results are also presented in this section. Section 4 is the Discussion, and the conclusions are presented in section 5.

2. Materials and Methods

2.1. MODIS Products

MODIS provides accurate land, ocean, and atmosphere products with high spatial resolution from at least four daily observations at most locations on the Earth's surface [*Justice et al*., 1998]. Table 1 provides the used MODIS products in this study. The MODIS TOA radiance product MOD021KM was first used to retrieve surface upwelling longwave radiation (LWUP) and then LWDN in conjunction with the MODIS atmospheric product MOD05. The MODIS geolocation product MOD03 was used to find the matchup between site-measured

Table 1. MODIS Version 5 Products Used in This Study

MODIS Product	Short Name	Spatial Resolution	Used Parameters
TOA radiance product	MOD021KM	1 km	TIR radiance for channel 29, 31, and 32
Geolocation product	MOD03	1 km	Geolocation and sensor viewing zenith angle
Atmospheric product	MOD05	1 km	Column water vapor derived from near-infrared measurements
Surface temperature and emissivity product	MOD11_L2	1 km	Quality control of land surface temperature and emissivity

LWDN and satellite-measured TOA radiance and CWV. The MODIS cloud product MOD35 is used to identify clear-sky pixels in producing the MODIS land surface temperature and emissivity (LST&E) product MOD11_L2. According to the studies of *Wan* [2008], it is still not possible to make a perfect cloud mask in all cases even when a series of spectral tests with multiple MODIS bands are used in the generation of MOD35, and cloud-contaminated LSTs are detected in the produced LST. One of the refinements of MOD11_L2 V5 is the removal of cloud-contaminated LSTs. Clear-sky identification using MOD11_L2 V5 is more effective than using MOD35. Thus, the quality control information of MOD11_L2 was used to identify clear-sky pixels.

2.2. Ground Measurements

The most popular instrument for measuring LWDN directly is the so-called "pyrgeometer." The actual spectral response function of the pyrgeometer covers a spectral range from approximately 3 μm to 50 μm and reaches the spectral range from 4 μm to 100 μm after calibration [*Wang and Dickinson*, 2013]. This type of infrared instrument is expensive and difficult to maintain when compared to currently used optical instruments that measure shortwave radiation. Thus, it is not routinely deployed at weather stations.

During the past two decades, several long-term ground-based observation networks that provide surface longwave radiation budget measurements have been established to support research communities. Ground-based measurements of LWDN are available publicly. Ground-measured LWDN data, which are collected at 62 globally distributed sites from 6 networks, were used to develop and validate the proposed hybrid method, including 9 sites from the AmeriFlux network [*Baldocchi et al*., 2001], 7 sites from the AsiaFlux network [*Baldocchi et al*., 2001], 29 sites from the Baseline Surface Radiation Network (BSRN) [*Ohmura et al*., 1998], 4 sites from the Coordinated Energy and Water Cycle Observations Project (CEOP) network [*Ma et al*., 2005], 7 sites from the FLUXNET network [*Baldocchi et al*., 2001], and 6 sites from the SURFRAD network [*Augustine et al*., 2000]. Figure 1 shows the distribution of sites. These sites cover regions with different land cover types and climates. Their latitudes vary from 69.01°S to 78.93°N, and their elevations range from 4 m to 5038.6 m, and Table 2 summarizes the latitude, longitude, elevation, land cover, climatic type, and observation period for each site.

2.3. Description of the Developed Hybrid Method

The general form of our hybrid method is as follows:

$$\mathrm{LWDN} = a_0 + a_1\mathrm{LWUP} + a_2\log(1+w) + a_3\log(1+w)^2 + a_4\mathrm{Rad29} \quad (1)$$

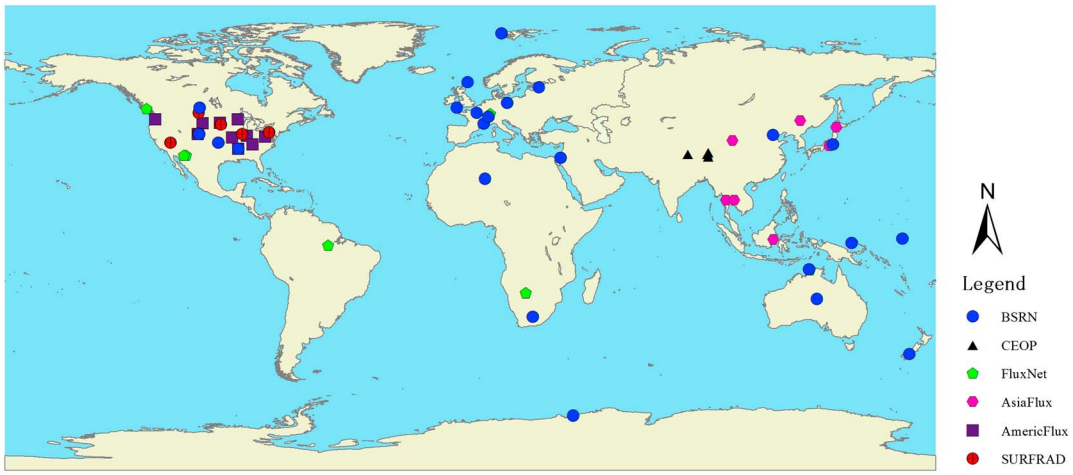

Figure 1. Distribution of 62 sites used in this paper.

Table 2. Descriptions of Site Conditions

Short Name	Full Name	Latitude (deg)	Longitude (deg)	Elevation (m)	Land Cover	Climatic Type[a]	Temporal Resolution	Time Period
Bondville[b]	Bondville, Illinois	40.05	−88.37	213	Cropland	Dfa	3 min	2003–2005
Boulder[b]	Boulder, Colorado	40.13	−105.24	1689	Grassland	BSk	3 min	2003–2005
Fort Peck[b]	Fort Peck, Montana	48.31	−105.10	634	Grassland	BSk	3 min	2003–2005
Desert Rock[b]	Desert Rock, Nevada	36.63	−116.02	1007	Desert	BWh	3 min	2003–2005
Penn State[b]	PennState, Pennsylvania	40.72	−77.93	376	Cropland	Dfb	3 min	2003–2005
Sioux Falls[b]	Sioux Falls, South Dakota	43.73	−96.62	473	Cropland	Dfa	3 min	2003–2005
US-Blk[c]	Black Hills	44.16	−103.65	1718	Evergreen needleleaf forest	Dfb	30 min	2004–2006
US-Bkg[c]	Brookings	44.35	−96.84	510	Grasslands	Dfa	30 min	2004–2006
US-CaV[c]	Canaan Valley	39.06	−79.42	994	Grasslands	Cfb	30 min	2004–2006
US-Goo[c]	Goodwin Creek	34.25	−89.87	87	Grasslands	Cfa	30 min	2003–2005
US-MMS[c]	Morgan Monroe State Forest	39.32	−86.41	275	Deciduous broadleaf forest	Cfa	30 min	2001–2003
US-WBW[c]	Walker Branch Watershed	35.96	−84.29	283	Deciduous broadleaf forest	Cfa	30 min	2003–2005
US-Wrc[c]	Wind River Crane Site	45.82	−121.95	371	Evergreen needleleaf forest	Csb	30 min	2003–2005
US-WCr[c]	Willow Creek	45.81	−90.08	520	Deciduous broadleaf forest	Dfb	30 min	2003–2005
US-MOz[c]	Missouri Ozark Site	38.74	−92.20	220	Deciduous broadleaf forest	Cfa	30 min	2003–2005
QHB[d]	Qinghai Flux Research Site	37.61	101.33	3250	Grasslands	BSk	15 min	2003–2004
MKL[d]	Mae Klong	14.58	98.84	231	Mix forest	Am	15 min	2003–2004
TMK[d]	Tomakomai Flux Research Site	42.74	141.52	140	Deciduous needleleaf forest	Dfb	15 min	2001–2003
BKS[d]	Bukit Soeharto	-0.86	117.04	20	Evergreen broadleaf forest	Af	15 min	2001–2002
FJY[d]	Fujiyoshidaforest Meteorology Research Site	35.45	138.76	1030	Deciduous needleleaf forest	Cfa	15 min	2000
LSH[d]	Laoshan	45.28	127.58	340	Deciduous needleleaf forest	Cfc	15 min	2002
SKR[d]	Sakaerat	14.49	101.92	543	Evergreen broadleaf forest	Aw	15 min	2001–2003
Amdo[e]	Amdo Tower	32.24	91.62	4695	Bare land	ET	60 min	2002–2004
BJ[e]	BJ Tower	31.37	91.90	4509	Bare land	ET	60 min	2002–2004
D105[e]	D105AWS	33.06	91.94	5038	Bare land	ET	60 min	2002–2004
Gaize[e]	Gaize	32.30	84.05	4416	Bare land	Dwb	60 min	2002–2004
BOU[f]	Boulder	40.05	−105.01	1577	Grasslands	BSk	1 min	2003–2005
CAR[f]	Carpentras	44.08	5.06	100	Cultivated	Csb	1 min	2003–2005
DAR[f]	Darwin	−12.43	130.89	30	Grasslands	Aw	1 min	2003–2005
LIN[f]	Lindenberg	52.21	14.12	125	Cultivated	Dfb	1 min	2003–2005
MAN[f]	Momote	−2.06	147.43	6	Grasslands	Af	1 min	2003–2005
NAU[f]	Nauru Island	−0.52	166.92	7	Rock	Af	1 min	2003–2005
NYA[f]	Ny-Ålesund	78.93	11.93	141	Tundra	ET	1 min	2003–2005
PAY[f]	Payerne	46.82	6.94	491	Cultivated	Dfb	1 min	2003–2005
REG[f]	Regina	50.21	−104.71	578	Cultivated	Dfb	1 min	2003–2005
E13[f]	Southern Great Plains	36.61	−97.49	318	Grasslands	Cfa	5 min	2003–2005
TAT[f]	Tateno	36.05	140.13	25	Grasslands	Cfa	1 min	2003–2005
DAA[f]	De Aar	−30.7	23.99	1287	Desert	BWk	5 min	2002–2004
SBO[f]	Sede Boqer	30.86	34.78	500	Desert	BWk	1 min	2003–2005
ASP[f]	Alice Springs	−23.80	133.89	547	Grasslands	BWh	1 min	2003–2005
BIL[f]	Billings	36.61	−97.52	317	Grasslands	Cfa	1 min	2003–2005
BON[f]	Bondville	40.07	−88.37	213	Grasslands	Dfa	3 min	2003–2005
BOS[f]	Boulder	40.125	−105.24	1689	Grasslands	Dfa	3 min	2003–2005
CAM[f]	Camborne	50.22	−5.32	88	Grasslands	Cfb	1 min	2003–2005
DRA[f]	Desert Rock	36.63	−116.02	1007	Desert	BWh	3 min	2003–2005
GCR[f]	Goodwin Creek	34.25	−89.87	98	Grasslands	Cfa	3 min	2003–2005

Table 2. (continued)

Short Name	Full Name	Latitude (deg)	Longitude (deg)	Elevation (m)	Land Cover	Climatic Type[a]	Temporal Resolution	Time Period
LAU[f]	Lauder	−45.045	169.869	250	Grassland	Cfb	3 min	2003–2005
SYO[f]	Syowa	−69.01	39.59	18	Ice	EF	3 min	2003–2005
LER[f]	Lerwick	60.14	−1.18	80	Grasslands	Cfb	1 min	2003–2005
PAL[f]	Palaiseau, SIRTA Observatory	48.71	2.21	156	Concrete	Cfb	1 min	2006
PSU[f]	Rock Springs	40.72	−77.93	376	Cultivated	Dfa	3 min	2003–2005
SXF[f]	Sioux Falls	43.73	−96.62	473	Grasslands	Dfa	3 min	2004–2006
TAM[f]	Tamanrasset	22.79	5.52	1385	Desert	BWh	1 min	2003–2005
TOR[f]	Toravere	58.25	26.46	70	Grasslands	Dfb	1 min	2003–2005
XIA[f]	Xianghe	39.75	116.96	32	Desert	Dwa	1 min	2005–2007
AU-How[g]	Howard Springs	−12.50	131.20	41	Savanna	Aw	30 min	2003–2005
BW-GhG[g]	Ghanzi Grass Site	−21.50	21.74	1161	Grassland	BSh	30 min	2003
BW-GhM[g]	Ghanzi Mixed Site	−21.20	21.75	1139	Savannas	BSh	30 min	2003
CA-Ca1[g]	BC-Campbell River 1949 Douglas-fir	49.87	−125.30	313	Evergreen needleleaf forest	Csb	30 min	2003–2005
DE-Har[g]	Hartheim	47.93	7.60	201	Mixed forests	Cfb	30 min	2005–2006
US-Wkg[g]	Walnut Gulch Kendall Grasslands	31.74	−109.94	1524	Grasslands	BSk	30 min	2004–2006
US-SRM[g]	Santa Rita Mesquite	31.82	−110.87	1118	Open shrublands	BSk	30 min	2004–2006
BR-Sa3[g]	Santarem-Km83-Logged Forest	−3.02	−54.97	100	Evergreen broadleaf forest	Am	30 min	2001–2003

[a]Koppen climate classification (https://en.wikipedia.org/wiki/K%C3%B6ppen_climate_classification).
[b]SURFRAD sites.
[c]AmeriFlux sites.
[d]AsiaFlux sites.
[e]CEOP sites.
[f]BSRN sites.
[g]FluxNet sites.

where *w* is the total column water vapor and Rad29 is the MODIS TOA radiance for channel 29. The primary considerations motivating the use of this formulation are as follows:

1. LWUP is the result of Earth-atmosphere interactions and equals the sum of the surface's self-emission and the LWDN reflected from the surface. Compared to LST, a commonly used indicator of Earth-atmosphere interactions [*Gupta et al*., 2010; *Zhou et al*., 2007], the hybrid method for estimating LWUP is easy to implement and has a high accuracy [*Nie et al*., 2016; *Wang et al*., 2009], while the LST estimate is prone to contamination by many factors such as clouds [*Wan*, 2008] and occasionally has large uncertainties [*Wang et al*., 2008]. LWUP was adopted as a proxy of air temperature at screening level to predict LWDN.
2. Water vapor is the major greenhouse gas in the atmosphere and shows the most prominent variation over short time scales. The column water vapor (CWV, also called total precipitable water vapor) and its vertical distribution are critical to LWDN. Previously, CWV was used as one of the predictors to calculate LWDN [*Gupta et al*., 2010; *Zhou et al*., 2007] and has been used for calculating the atmospheric downward and upwelling radiance at the window region in the single channel algorithm for LST retrieval [*Jimenez-Munoz and Sobrino*, 2003; *Qin and Karnieli*, 2001]. Therefore, we used the same form of CWV as that used by *Zhou et al*. [2007] to predict LWDN.
3. The weighting function of MODIS water vapor sounding channel 29 peaks at the surface. The TOA radiance of MODIS channel 29 can represent the water vapor at the surface to some extent. Thus, we used the TOA radiance from MODIS channel 29 to characterize the water vapor in the lower atmosphere in this study.

Figure 2 shows a flowchart describing the proposed hybrid method for estimating LWDN. First, spatial and temporal matching between satellite data and site measurements was implemented through three steps: (1) spatial matching: the position of a site in the image was found by spatial matching using the site's coordinates and MOD03; (2) clear-sky identification: if the corresponding LST had the highest quality, the

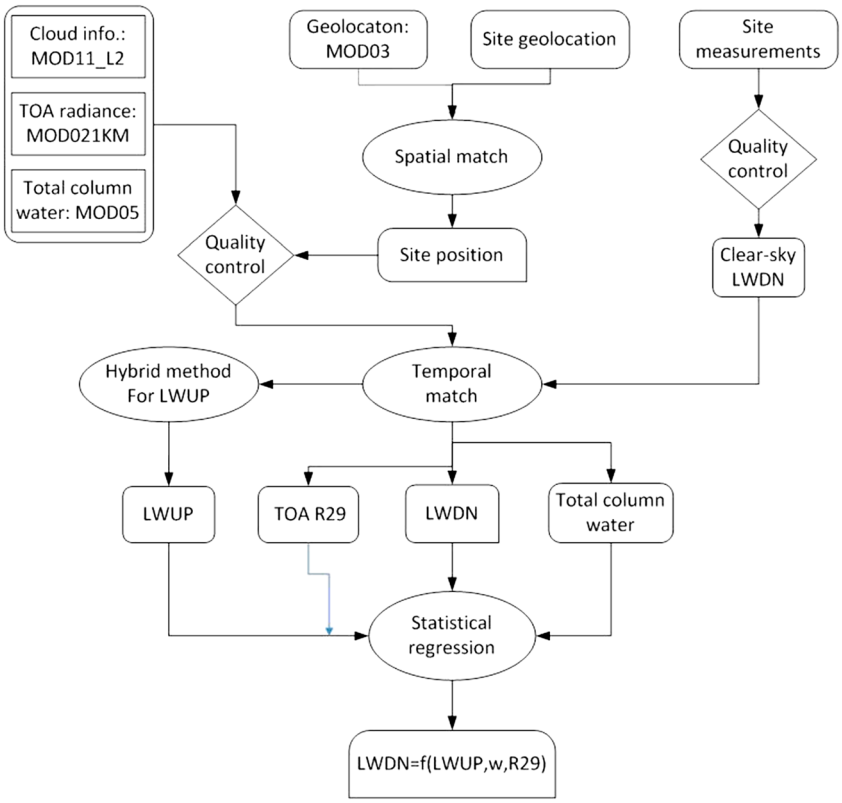

Figure 2. Flowchart showing the efficient hybrid method for LWDN estimation.

pixel was identified as clear sky; the clear sky of the site was determined based on fractional cloud cover, which was calculated using $c = 1 - S_{measured}/S_{calculated}$, where $S_{measured}$ is the ground-measured downward solar radiation, and $S_{calculated}$ is the theoretical downward clear-sky solar radiation for the period [*Crawford and Duchon*, 1999]; when c was less than 0.05, the sky was considered to be clear; and (3) temporal matching. The temporally matched site measurements were found using the nearest-neighbor method based on the overpass time of the satellite and the time of site measurements. For example, the time difference between the satellite overpass time and the time of ground measurements is required to be less than 15 min given that the temporal resolution of the site measurements is 30 min. Through these steps, we obtained high-quality, spatially and temporally matched clear-sky samples. The samples were randomly divided into two parts. Two thirds of the samples were used to develop the proposed hybrid method, and one third of the samples were used to test the hybrid method. Then the LWUP values were derived from the MODIS thermal infrared (TIR) TOA channel radiance of channels 29, 31, and 32 using the algorithm described by *Cheng and Liang* [2016]. Finally, statistical regression was used to determine the coefficient in equation (1) using two thirds of the samples.

3. Results Analysis

3.1. Evaluating the Accuracy of LWUP Estimation

One of the inputs to the proposed hybrid method is the LWUP, whose accuracy will certainly affect the accuracy of the LWDN estimates. Among the sites used, 32 sites have LWUP measurements. The hybrid method for estimating LWUP was validated using these data. The validation results are shown in Figure 3. When the LWUP was smaller than 500 W/m^2, no obvious underestimation or overestimation appeared in the scatterplot, while a few samples with positive bias were noted when the LWUP values were larger than 500 W/m^2. These samples belonged to FLUXNET sites US-SRM and US-Wkg. The exact reasons for this inconsistency are not clear. The bias and RMSE values were 0.569 W/m^2 and 24.291 W/m^2, which are consistent

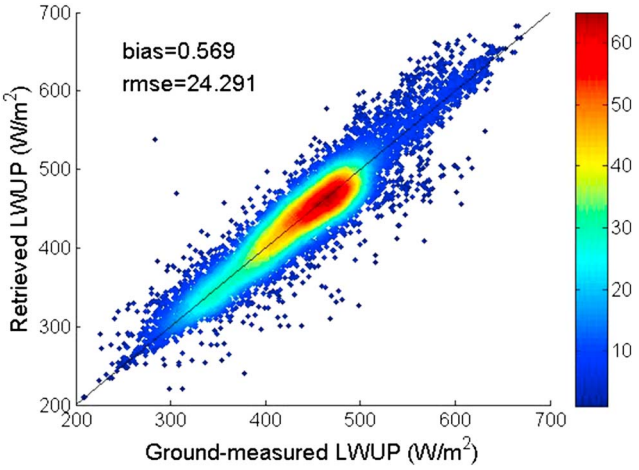

Figure 3. Validation results of the hybrid method for LWUP estimation.

with the results of validation during the algorithm development stage [*Cheng and Liang*, 2016]. Note that there is an abnormal point in the upper left corner of Figure 3. This point belongs to the samples from the CEOP site Gaize. The TOA radiance values for channels 29, 31, and 32 used to calculate LWUP are quite large and correspond to an LWUP value of 538.294 W/cm^2, whereas the observed LWUP is 283.69 W/cm^2. Visual inspection of the satellite image indicates it is clear. The LWDN derived using calibrated clear-sky parameterization method of *Prata* [1996] with ground-measured air temperature and relative humidity is consistent with the ground-measured LWDN. It seems the observation data are rational. The satellite data may be disturbed, but the specific reason remains unknown.

3.2. Results for LWDN Estimation

Using the method described in section 2.3, we obtained 16,700 samples and derived the following linear function by linear regression

$$\mathrm{LWDN} = 108.954 + 0.112\mathrm{LWUP} + 120.984\log(1+w) - 3.692\log(1+w)^2 + 5.5\mathrm{Rad29} \quad (2)$$

The fitting results are shown in Figure 4. The correlation coefficient was 0.951, and the bias and RMSE were 0.081 W/m^2 and 20.929 W/m^2. The LWDN values were overestimated at the low end of the LWDN range, where the ground-measured LWDN values were approximately 150 W/m^2. However, the fraction of samples affected was very small. The few points that were underestimated and lie below the 1:1 line may be affected by undetected cloud contamination.

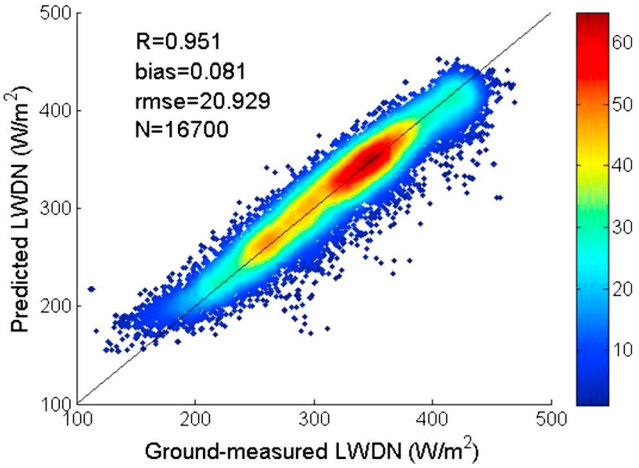

Figure 4. Results of fitting the proposed hybrid method.

To investigate the influence of the independent variables (CWV, LWUP, and Rad29) on the LWDN estimation using equation (2), we plot the scatters of the residuals (predicted LWDN minus ground-based measurements of LWDN) and the independent variables, which are shown in Figure 5. Although the number of outliers below −50 W/m^2 was larger than the number above 50 W/m^2, there were no clearly significant trends between the fitting residues and each independent variable. Therefore, the effect of CWV, LWUP, and Rad29 on the accuracy of LWDN estimation is not significant.

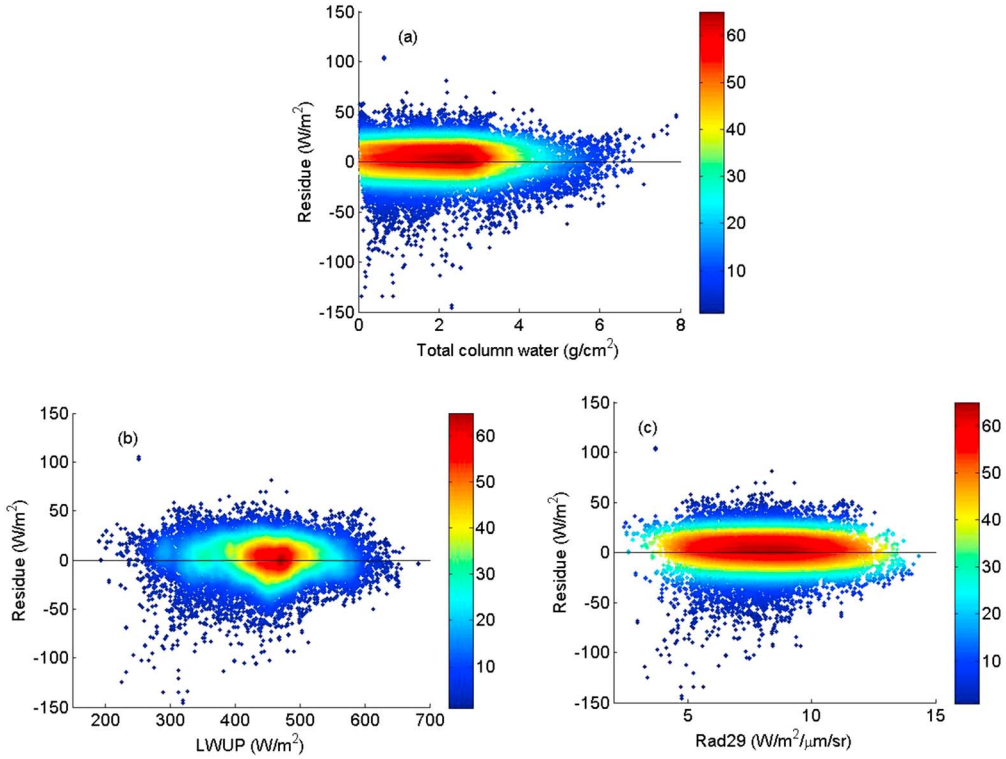

Figure 5. Scatterplots of residuals versus (a) CWV, (b) LWUP, and (c) the radiance of MODIS channel 29.

3.3. Error Analysis

According to the error propagation law, the uncertainty can be calculated as

$$\sigma_{\mathrm{LWDN}} = \left(0.112^2\sigma_{\mathrm{LWUP}}^2 + \left(\frac{120.984}{1+w}\right)^2\sigma_w^2 + \left(\frac{2{*}3.692\log(1+w)}{1+w}\right)^2\sigma_w^2 + 5.5^2\sigma_{\mathrm{Rad29}}^2\right)^{1/2} \quad (3)$$

where σ_{LWUP} and σ_w are the uncertainties of LWUP and CWV, and σ_{Rad29} is the calibration error of the MODIS emissive bands. In this study σ_{LWUP} was set as 24.291 W/m^2, according to the validation results for LWUP in section 3.1, σ_w was set to a value of 0.2 g/cm^2 [*Mao et al.*, 2010; *Prasad and Singh*, 2009], and the calibration accuracy of MODIS emissive was assigned as 0.5% [*Chang and Xiong*, 2011; *Xiong et al.*, 2009]. The uncertainty was 8.851 W/m^2 assuming w equals the mean value from the training data set. The uncertainty was 21.224 W/m^2 if w equals 0.5 g/cm^2. The absolute error of the LWDN estimate can be calculated as

$$\varepsilon = \left(RMSE^2 + \sigma_{\mathrm{LWDN}}^2\right)^{1/2} \quad (4)$$

Substituting the corresponding values into equation (4), the absolute errors were 22.724 W/m^2 and 29.808 W/m^2 when w equals 0.2 g/cm^2 and 0.5 g/cm^2, respectively.

The Monte Carlo (MC)-based uncertainty and sensitivity analysis software SimLab was used to conduct uncertainty and sensitivity analysis. MC-based uncertainty and sensitivity analyses are based on performing multiple model evaluations with probabilistically selected model inputs and then using the results of these evaluations to determine (1) the uncertainty in model predictions and (2) the input variables that give rise to this uncertainty. In this study, a global sensitivity analysis method, the Fourier amplitude sensitivity test (FAST), was used for sampling and sensitivity analysis [*Saltelli et al.*, 1999]. The FAST approach is based on performing numerical

Table 3. FAST-Calculated Model Uncertainty of Equation (2) and the FAST Sensitivity Indices of the First Order for Each Input in Equation (2)

Uncertainty (W/m^2)		FAST Sensitivity Indices of the First Order		
Mean	Standard	LWUP	log(1 + w)	Rad29
315.359	51.735	0.027	0.901	0.035

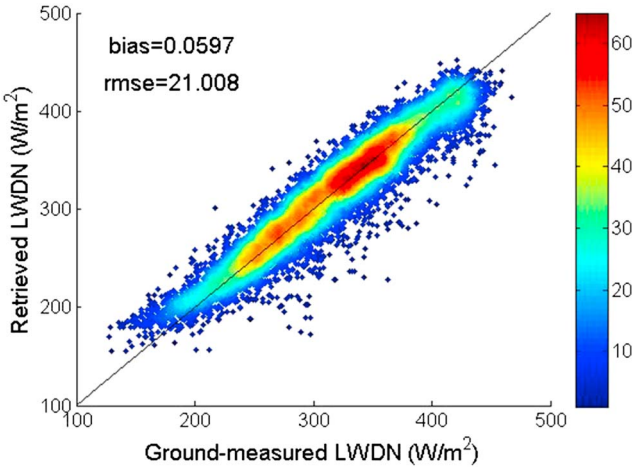

Figure 6. Validation results of the proposed hybrid method.

calculations to obtain the expected value and variance of a model prediction. The basis of this calculation is a transformation that converts a multidimensional integral over all uncertain model inputs to a one-dimensional integral. The first-order FAST sensitivity indices are calculated using the terms of a Fourier decomposition of the model output. Given the probability distribution function of each input, we generated a large number of samples with the FAST sampling technique and then used FAST to perform a sensitivity analysis using equation (2). The result is presented in Table 3. We can see clearly from Table 3 that the contribution of each input to the total variance was different. The most important factor was $\log(1+w)$ in equation (2), which captures 90.1% of the output variance. The uncertainty of LWDN as estimated by equation (2) was $315.359 \pm 51.735\ \mathrm{W/m^2}$, which mean the probability that LWDN lies in [160.154, 470.564] is 0.9974 the 3σ principle of normal distribution.

3.4. Validation

As described in section 2.3, one third of the samples was extracted and used to validate the proposed hybrid method. Figure 6 shows the validation results. The bias and RMSE were $0.0597\ \mathrm{W/m^2}$ and $21.008\ \mathrm{W/m^2}$, which agree well with the results of error analysis. As in Figure 4, the LWDN values were overestimated at the low end of the LWDN range. Using 15 sites from SURFRAD, CEOP-Tibet, and AsiaFlux, *Gui et al.* [2010] validated three mainstream longwave flux data sets and the LWDN estimation method of *Wang et al.* [2009]. According to the validation results, the biases of clear-sky LWDN and LWDN from Global Energy and Water Cycle Experiment-Surface Radiation Budget (GEWEX-SRB), International Satellite Cloud Climatology Project - Flux Data (ISCCP-FD), and Clouds and Earth Radiant Energy System - Gridded Radiation Fluxes and Clouds (CERES - FSW), as estimated by the nonlinear model of *Wang et al.* [2009], were $-20.4\ \mathrm{W/m^2}$, $4.4\ \mathrm{W/m^2}$, $-10.7\ \mathrm{W/m^2}$, and $-9.2\ \mathrm{W/m^2}$. The corresponding RMSE values were $20.6\ \mathrm{W/m^2}$, $28.6\ \mathrm{W/m^2}$, $19.2\ \mathrm{W/m^2}$, and $21.0\ \mathrm{W/m^2}$. Compared to the above validation results, our method is more accurate.

As shown in Table 4, we also calculated the validation results separately for each network. For high-elevation CEOP sites, the bias and RMSE were $13.869\ \mathrm{W/m^2}$ and $24.006\ \mathrm{W/m^2}$. Regarding the remaining networks, the absolute value of the bias was approximately $10\ \mathrm{W/m^2}$, and the RMSE was approximately $20\ \mathrm{W/m^2}$, with the exception of AsiaFlux. The validation results of the BSRN and SURFRAD networks were better than those of the other networks. We speculate that one of the primary reasons may be the higher temporal resolution of ground measurements. For example, the temporal resolution of SURFRAD is 3 min and the temporal resolution of most BSRN sites is 1 min, whereas the temporal resolution of CEOP is 60 min. Temporal mismatches between ground measurements and satellite overpasses will inevitably introduce additional errors in the validation.

4. Discussion

4.1. Possible Reasons for LWDN Overestimation

The overestimated samples in Figures 4 and 6 corresponded to the high-elevation sites, with surface elevations greater than 3000 m, that had extremely low CWV. Here we took sites QHB and D105 from the

Table 4. Validation Results for Each Network

Network	Ameriflux	Asiaflux	BSRN	CEOP	Fluxnet	SURFRAD
Bias ($\mathrm{W/m^2}$)	−3.452	−15.386	1.420	13.869	−7.722	5.389
RMSE($\mathrm{W/m^2}$)	25.066	28.909	19.233	24.066	23.801	17.531

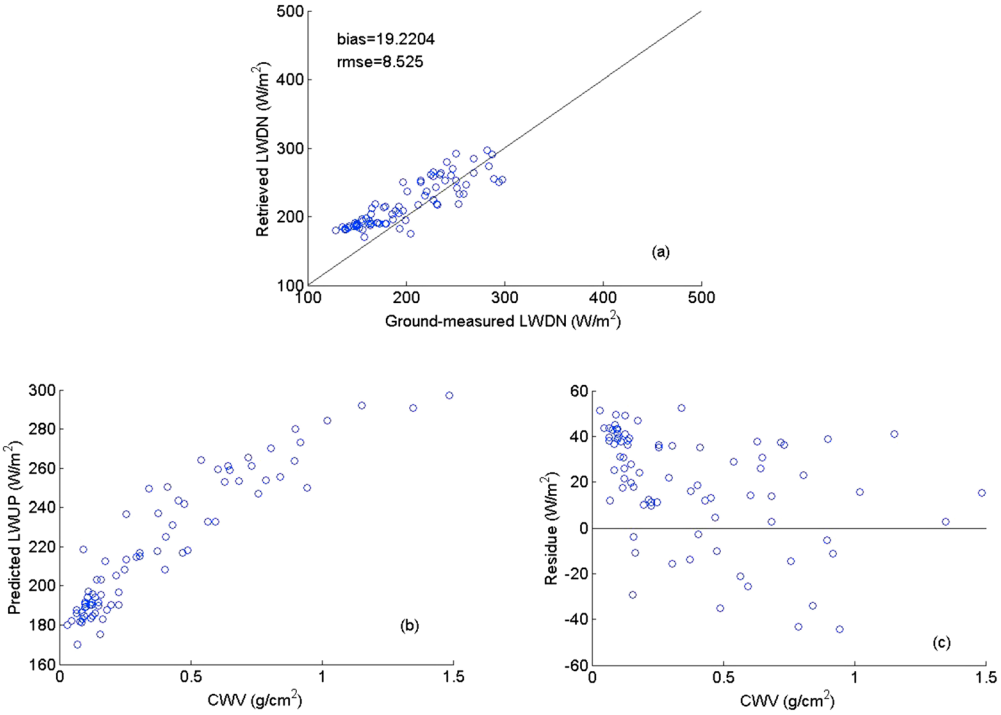

Figure 7. Validation results for site QHB from the AsiaFlux network. (a) Scatterplot, (b) LWDN versus CWV, and (c) residuals versus CWV.

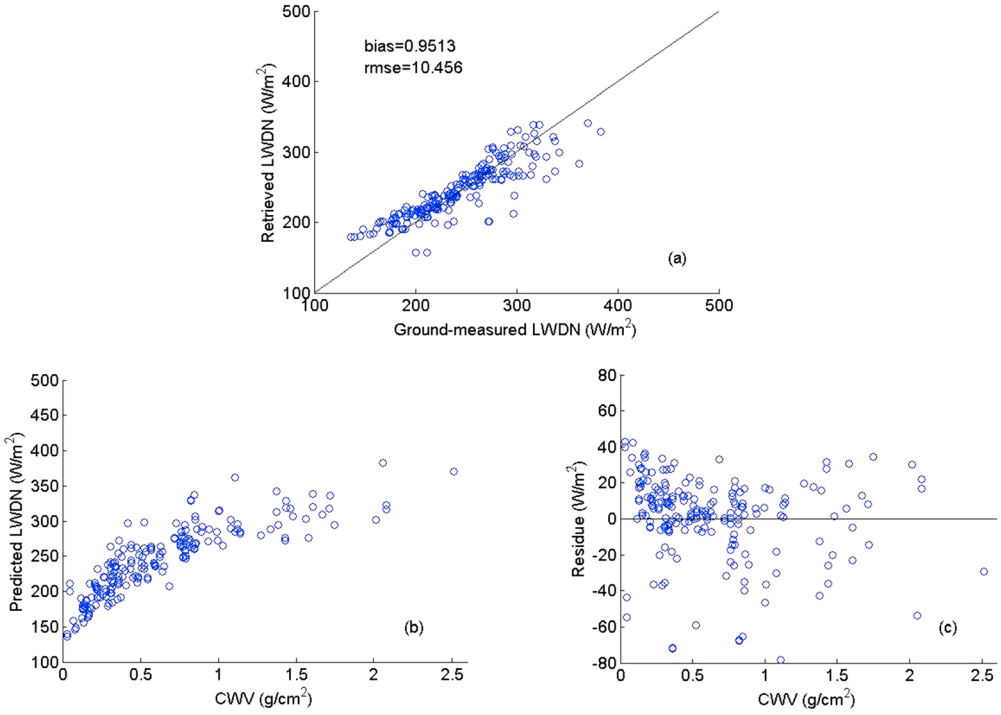

Figure 8. Validation results for site D105 from the CEOP network. (a) Scatterplot, (b) LWDN versus CWV, and (c) residuals versus CWV.

Table 5. Accuracy of the Proposed Hybrid Method for Different Land Cover Types

Land Cover	Bare Land	Cropland	Desert	Forest	Grassland
NO. of sites	4	8	6	16	27
bias	13.869	6.204	−0.752	−11.977	3.251
RMSE	24.066	17.168	16.928	23.058	20.344

AsiaFlux and CEOP networks as examples to explore the possible reasons. As shown in Figure 7, the bias was less than 1 W/m^2 and RMSE was 10.456 W/m^2 at site QHB, but LWDN was obviously overestimated when ground-based measurements of LWDN were less than 200 W/m^2. The corresponding CWV was less than 0.5 g/cm^2, and most of the residuals were positive. We also examined site D105, which has low-CWV values, and similar results were obtained (Figure 8).

According to equation (2) and the results of our sensitivity analysis (Table 3), we can see that small perturbations in the MODIS CWV data product introduced large residuals. The MODIS CWV data product, which is derived from near-infrared measurements, had a high correlation with GPS measurements in southern Tibet but generally tended to overestimate water vapor under clear-sky conditions [*Lu et al*., 2011]. We also used ground-based measurements of LWUP to predict LWDN at sites QHB and D105, and the residuals stayed almost the same. Therefore, we conclude that CWV may be one of the factors that is responsible for this overestimation. This result is consistent with the study of *Naud et al*. [2013], who claimed that the drier the atmosphere is, the greater the impact of a small change in humidity on LWDN. Another reason may be that our method does not work well under high-elevation conditions.

4.2. The Effects of Land Cover, Climatic Type, and Surface Elevation

In this section, factors such as land cover, climatic type, and surface elevation that may affect or modulate Earth-atmosphere interactions were also investigated. First, the land surface was divided into five primary land cover types. The performance of the proposed hybrid method was subsequently evaluated.

The accuracy of the LWDN estimates for different land cover types is shown in Table 5. The bare land sites all came from the CEOP network; their bias and RMSE values were the same. The forest sites had the largest negative bias of −11.977 W/m^2. The forest sites came from the AmeriFlux, AsiaFlux, and FLUXNET networks. These three networks all had negative biases, as shown in Table 4. The performance over the other land cover types was satisfactory; the bias was less than 6.204 W/m^2 and the RMSE was approximately 20 W/m^2.

The accuracy of the LWDN estimates for different climatic types is shown in Table 6. The LWDN was underestimated for sites that had extremely high CWV and tropical rainforest (af) or tropical monsoon climates (am). The ground-based measurements of LWDN lay at one end of the range of LWDN values and varied from 400 to 450 W/m^2. The bias of af and am were −13.164 W/m^2 and −26.743 W/m^2, and the corresponding RMSE values were 26.339 W/m^2 and 30.353 W/m^2. The bias for the remaining eight climatic types was less than 7.432 W/m^2, and the RMSE was approximately 20 W/m^2.

The sites were classified into four groups according to their surface elevations (<500 m, 500–1000 m, 1000–3000 m, and >3000 m). The performance of the hybrid method is provided in Table 7. There was no trend with respect to surface altitude. The bias was less than 10 W/m^2, and the RMSE was approximately 20 W/m^2, for all elevation groups.

Generally, there is no significant trend in LWDN with respect to land cover, climatic type, and surface elevation, except for the observed overestimation and underestimation at the low and high ends of the range of LWDN, respectively.

Table 6. Accuracy of the Proposed Hybrid Method for Different Climatic Types

	Climatic Type											
	af	am	aw	bs	bw	af	cf	cs	df	dw	et	cf
No. of sites	3	2	3	8	6	3	15	3	16	2	4	15
Bias	−13.164	−26.743	3.509	6.423	−1.315	−13.164	0.779	−7.097	3.181	6.957	5.764	0.779
RMSE	26.339	30.353	22.103	22.039	16.933	26.339	20.530	19.832	19.442	17.418	29.139	20.530

Table 7. The Accuracy of the New Hybrid Method for Different Surface Elevations

Altitude	<500	500–1000	1000–3000
No. of sites	37	7	13
Bias	−2.886	8.372	2.337
RMSE	20.525	23.952	19.644

4.3. A Complementary Method

To improve the LWDN estimation over high-elevation areas with extremely low CWV and tropical climatic types with extremely high CWV, we first attempted to retrieve the LWDN using traditional parameterizations. We extracted the required clear-sky samples from the ground-based measurements in the six networks (Table 2). The extracted samples were randomly divided into two parts; two thirds of the samples were used to calibrate the selected seven commonly used parameterizations; one third was used to test the performance of the methods. The overall accuracy of these methods was lower than that of our hybrid method in this study. In addition, their accuracy at high-elevation, low-CWV sites and for the af and am climatic types was also lower than that of this study.

Another choice may be the data integration method. For example, Zhang et al., improved the accuracy of incident solar radiation by merging satellite retrieval and ground-based measurements using smoothing splines [*Zhang et al*., 2016]. The overestimation of lower incident solar radiation and underestimation of high incident solar radiation were appropriately corrected. The overestimation and underestimation of LWDN may be corrected by merging satellite retrieval and ground-measured LWDN. However, this method requires many well-distributed high-quality ground-based measurements, but sites containing LWDN measurements are highly scarce.

The LWDN is sensitive to CWV at high elevations [*Naud et al*., 2012]. Using the same data as section 3.2, we constructed a scatterplot of LWDN versus CWV. As shown in Figure 9, there was a power relationship between LWDN and CWV. The derived power function was as follows:

$$\mathrm{LWDN} = 283.157w^{0.245} \tag{5}$$

The correlation coefficient was 0.919, the bias was $-1.035\ \mathrm{W/m^2}$, and the RMSE was $25.80\ \mathrm{W/m^2}$. The results of fitting equation (5) were not as good as those of equation (2) because only CWV was used. The LWDN stayed almost the same when CWV was larger than $6\ \mathrm{g/cm^2}$, so the derived relationship failed. The divergence of the samples at the ends of the curve ($\mathrm{CWV} > 0\ \mathrm{g/cm^2}$ and $\mathrm{CWV} < 6\ \mathrm{g/cm^2}$) was much weaker than in the middle part ($\mathrm{CWV} > 0.5\ \mathrm{g/cm^2}$ and $\mathrm{CWV} < 4\ \mathrm{g/cm^2}$), which indicated that better results were desired when CWV was low or high.

When equation (5) was applied to the high-elevation sites QHB and D105, we obtained the results shown in Figure 10. The overestimation disappeared. Table 8 provides the results of comparison between equations (2) and (5) for high-elevation sites. The error for the high-elevation sites greatly improved; the bias decreased from $9.407\ \mathrm{W/m^2}$ to $-0.924\ \mathrm{W/m^2}$, and the RMSE decreased from $23.919\ \mathrm{W/m^2}$ to $19.895\ \mathrm{W/m^2}$. Checking the CWV of the high-elevation sites, we found that approximately 70% of the CWV values were less than $0.5\ \mathrm{g/cm^2}$, which demonstrated that equation (5) can work effectively over areas with extremely low CWV.

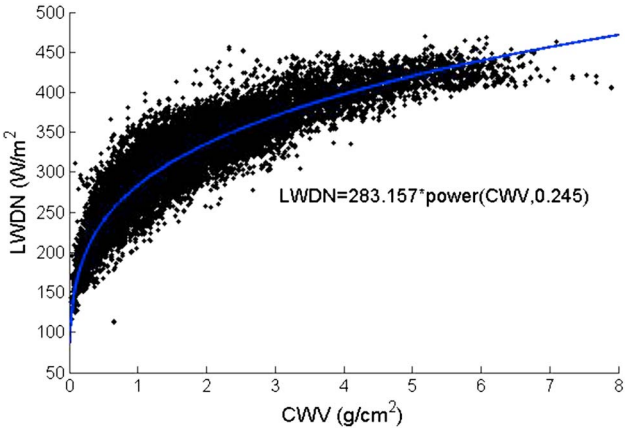

Figure 9. Scatterplot of LWDN and CWV.

The accuracy for af climatic types improved if equation (5) was used to estimate their LWDN. The bias

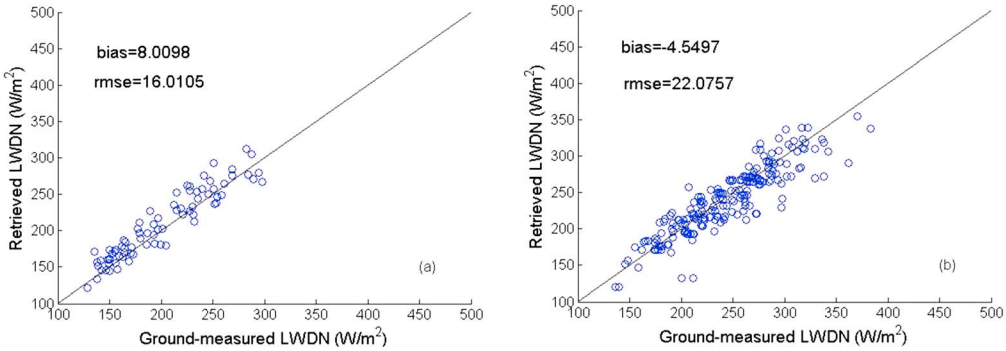

Figure 10. Comparison of ground-based measurements of LWDN and those calculated by equation (5) at sites (a) D105 and (b) QHB.

decreased from −13.164 W/m^2 to −4.824 W/m^2, and the RMSE decreased from 26.339 W/m^2 to 22.858 W/m^2. On the other hand, the accuracy for am climatic types was only partially improved, because over 75% of the CWV values associated with the af climatic type lay between 4 g/cm^2 and 6 g/cm^2, while the corresponding proportion for the am climatic type was 50%.

5. Conclusion

This study proposes an efficient hybrid method for estimating 1 km spatial resolution, instantaneous clear-sky LWDN values from MODIS thermal infrared observations, and the MODIS near-infrared CWV data product. The LWDN was formulated as a nonlinear function of LWUP estimated from the MODIS TOA radiance of channels 29, 31, and 32; CWV; and the MODIS TOA radiance of channel 29. The proposed hybrid method has an explicit physical meaning and is easy to implement. The spatially and temporally matched samples extracted from the ground-based measurements collected at 62 globally distributed sites of six networks and the MODIS data were randomly divided into two parts to develop and validate the hybrid method, respectively. Two thirds of the matched data were used to determine the coefficients of the hybrid method. The correlation coefficient was 0.951, and the bias and RMSE were 0.081 W/m^2 and 20.929 W/m^2. A comprehensive error analysis was conducted. The absolute errors of LWDN retrieval were 22.724 W/m^2 and 29.808 W/m^2, when the retrieval errors of CWV were 0.2 and 0.5 g/cm^2, respectively. The most important factor was associated with CWV, which captures 90.1% of the output variance. The uncertainty of the proposed LWDN estimation method was 315.359 ± 51.735 W/m^2. The proposed hybrid method was validated using one third of the matched data. The bias and RMSE were 0.0597 W/m^2 and 21.008 W/m^2, and the performance of our method is superior to the results of methods that estimate LWDN using MODIS data from the literature.

The drawback of our method is that LWDN is overestimated for high-elevation areas with extremely low CWV (CWV < 0.5 g/cm^2) and underestimated for tropical climatic types with extremely high CWV. A power function relating LWDN and CWV was derived and used as a complementary method to address these circumstances. The overestimation was overcome, and the accuracy was greatly improved; the bias and RMSE decreased from 9.407 W/m^2 and 23.919 W/m^2 to −0.924 W/m^2 and 19.895 W/m^2. The underestimation was also alleviated, and the error was reduced.

The hybrid method is being used to produce a global 1 km instantaneous clear-sky LWDN product from 2000 to 2016. Future efforts will focus on developing methods to estimate instantaneous cloudy-sky LWDN from MODIS data and estimating daily and monthly averaged LWDN using instantaneous LWDN under both clear-sky and cloudy-sky conditions.

Table 8. Results of Comparing Equations (2) and (5) for Sites at High Elevation and With the af and am Climatic Types[a]

Site Type	High Elevation	af	am
No. of sites	5	3	2
Bias	9.407(−0.924)	−13.164 (−4.824)	−26.743 (−20.299)
RMSE	23.919(19.895)	26.339 (22.858)	30.353 (26.3834)

[a]The values in the parentheses show the results of applying equation (5).

Acknowledgments

The MODIS data were obtained from http://reverb.echo.nasa.gov/reverb/. The Ameriflux data were downloaded from http://ameriflux.lbl.gov/, the Asiaflux data were downloaded from https://db.cger.nies.go.jp/asiafluxdb/, the CEOP data were downloaded from http://aan.suiri.tsukuba.ac.jp, the fluxnet data were downloaded from http://daac.ornl.gov/get_data.shtml, and the SURFRAD data were downloaded from http://www.srrb.noaa.gov, respectively. The SimLab was downloaded from http://ipsc.jrc.ec.europa.eu/?id=756. This work was partly supported by the National Natural Science Foundation of China via grants 41371323 and 41331173, the National High Technology Research and Development Program of China via grant 2013AA122801, and the Beijing Higher Education Young Elite Teacher Project via grant YETP0233.

References

Augustine, J. A., J. J. DeLuisi, and C. N. Long (2000), SURFRAD-A national surface radiation budget network for atmospheric research, *Bull. Am. Meteorol. Soc.*, *81*(10), 2341–2357.

Baldocchi, D., et al. (2001), FLUXNET: A new tool to study the temporal and spatial variability of ecosystem-scale carbon dioxide, water vapor, and energy flux densities, *Bull. Am. Meteorol. Soc.*, *82*, 2415–2434.

Brunt, D. (1932), Notes on radiation in the atmosphere, *Q. J. R. Meteorol. Soc.*, *58*, 389–420.

Brutsaert, W. (1975), On a derivable formula for long-wave radiation from clear skies, *Water Resour. Res.*, *11*, 742–744, doi:10.1029/WR011i005p00742.

Carmona, F., R. Rivas, and C. Caselles (2014), Estimation of daytime downward longwave radiation under clear and cloudy skies conditions over a sub-humid region, *Theor. Appl. Climatol.*, *115*, 281–295.

CEOS, and WMO (2000), CEOS/WMO online database: Satellite system and requirements, The Committee on Earth Observation Satellites, The World Meteorological Organization.

Chang, T., and X. Xiong (2011), Assessment of MODIS thermal emissive band on-orbit calibration, *IEEE Trans. Geosci. Remote Sens.*, *49*(6), 2415–2425.

Cheng, J., and S. Liang (2016), Global estimates for high spatial resolution clear-sky land surface upwelling longwave radiation from MODIS data, *IEEE Trans. Geosci. Remote Sens.*, *54*(7), 4115–4129, doi:10.1109/TGRS.2016.253765.

Crawford, T. M., and C. E. Duchon (1999), An improved parameterization for estimating effective atmospheric emissivity for use in calculating daytime downwelling longwave radiation, *J. Appl. Meteorol.*, *38*, 474–480.

Diak, G. R., W. L. Bland, J. R. Mecikalski, and M. C. Anderson (2005), Satellite-based estimates of longwave radiation for agricultural applications, *Agric. For. Meteorol.*, *103*(4), 1517–1531.

Dubayah, R. (1995), An approach to the estimation of surface net radiation in mountain area using remote sensing and digital terrain data, *Theor. Appl. Climatol.*, *52*, 55–68.

Ellingson, R. G. (1995), Surface longwave fluxes from satellite observations: A critical review, *Remote Sens. Environ.*, *51*, 89–97.

Gui, S., S. Liang, and L. Li (2010), Evaluation of satellite-estimated surface longwave radiation using ground-based observations, *J. Geophys. Res.*, *115*, D18214, doi:10.1029/2009JD013635.

Gupta, S. K., D. P. Kratz, and A. C. Wilber (2004), Validation of parameterized algorithms used to derive TRMM-CERES surface radiative fluxes, *J. Atmos. Oceanic Technol.*, *21*(5), 742–752.

Gupta, S. K., D. P. Kratz, P. W. Stackhouse, A. C. Wilber, T. Zhang, and V. E. Sothcott (2010), Improvement of surface longwave flux algorithms used in the CERES processing, *J. Appl. Meteorol. Climatol.*, *49*, 1579–1589.

Idso, S. B. (1968), An analysis of the heating coefficient concept, *J. Appl. Meteorol.*, *7*, 716–717.

Iziomon, M. G., H. Mayer, and A. Matzarakis (2003), Downward atmospheric longwave irradiance under clear and cloudy skies: Measurement and parameterization, *J. Atmos. Sol. Terr. Phys.*, *65*, 1107–1116.

Jimenez-Munoz, J. C., and J. A. Sobrino (2003), A generalized single-channel method for retrieving land surface temperature from remote sensing data, *J. Geophys. Res.*, *108*(D22), 4688, doi:10.1029/2003JD003480.

Justice, C. O., et al. (1998), The Moderate Resolution Imaging Spectroradiometer (MODIS): Land remote sensing for global change research, *IEEE Trans. Geosci. Remote Sens.*, *36*(4), 1228–1249.

Lee, H.-T. (1993), *Development of a Statistical Technique for Estimating the Downward Longwave Radiation at the Surface From Satellite Observations*, Univ. of Maryland, College Park.

Lee, H.-T., and R. G. Ellingson (2002), Development of a nonlinear statistical method for estimating the downward longwave radiation at the surface from satellite observations, *J. Atmos. Oceanic Technol.*, *19*, 1500–1515.

Liang, S., W. Kustas, G. Schaepman-Strub, and X. Li (2010a), Impacts of climate change and land use change on land surface radiation and energy budgets, *IEEE J. Sel. Top. Earth Obs. Remote Sens.*, *3*(3), 219–224.

Liang, S., K. Wang, X. Zhang, and M. Wild (2010b), Review of estimation of land surface radiation and energy budgets from ground measurements, remote sensing and model simulation, *IEEE J. Sel. Top. Earth Obs. Remote Sens.*, *3*(3), 225–240.

Lu, N., J. Qin, K. Yang, Y. Gao, X. Xu, and T. Koike (2011), On the use of GPS measurements for Moderate Resolution Imaging Spectrometer precipitable water vapor evaluation over southern Tibet, *J. Geophys. Res.*, *116*, D23117, doi:10.1029/2011JD016160.

Ma, Y., S. Fan, H. Ishikawa, O. Tsukamoto, T. Yao, T. Koike, H. Zuo, Z. Hu, and Z. Su (2005), Diurnal and inter-monthly variation of land surface heat fluxes over the central Tibetan Plateau area, *Theor. Appl. Climatol.*, *80*, 259–273.

Mao, K. B., H. Li, D. Hu, J. Huang, Z. Li, and J. Wang (2010), Estimation of water vapor content in near-infrared bands around 1 μm from MODIS data by using RM-NN, *Opt. Express*, *18*(9), 9542–9554.

Monteith, J. L., and G. Szeicz (1961), The radiation balance of bare soil and vegetation, *Q. J. R. Meteorol. Soc.*, *87*, 1–18.

Naud, C. M., J. R. Miller, and C. Landry (2012), Using satellites to investigate the sensitivity of longwave downward radiation to water vapor at high elevations, *J. Geophys. Res.*, *117*, D05101, doi:10.1029/2011JD016917.

Naud, C. M., Y. Chen, I. Rangwala, and J. R. Miller (2013), Sensitivity of downward longwave surface radiation to moisture and cloud changes in a high-elevation region, *J. Atmos.*, *118*, 10,072–10,081.

Nie, A., Q. Liu, and J. Cheng (2016), Estimating clear-sky land surface longwave upwelling radiation from MODIS data using a hybrid method, *Int. J. Remote Sens.*, *37*(8), 1747–1761.

Ohmura, A., et al. (1998), Baseline Surface Radiation Network (BSRN/WCRP): New precision radiometry for climate research, *Bull. Am. Meteorol. Soc.*, *79*, 2115–2136.

Prasad, A. K., and R. P. Singh (2009), Validation of MODIS Terra, AIRS, NCEP/DOE AMIP-II Reanalysis-2, and AERONET Sun photometer derived integrated precipitable water vapor using ground-based GPS receivers over India, *J. Geophys. Res.*, *114*, D05107, doi:10.1029/2008JD011230.

Prata, A. J. (1996), A new long-wave formula for estimating downward clear-sky radiations at the surface, *Q. J. R. Meteorol. Soc.*, *122*, 1127–1151.

Qin, Z., and A. Karnieli (2001), Mono-window algorithm for retrieving land surface temperature from Landsat TM data and its application to the Israel-Egypt border region, *Int. J. Remote Sens.*, *22*(18), 3719–3746.

Saltelli, A., S. Tarantola, and K. Chan (1999), A quantitative model-independent method for global sensitivity analysis of model output, *Technometrics*, *41*, 39–56.

Schmetz, J. (1989), Towards a surface radiation climatology: Retrieval of downward irradiances from satellites, *Atmos. Res.*, *23*(3-4), 287–321.

Smith, W. L., and H. M. Woolf (1983), Geostationary satellite sounder (VAS) observations of longwave radiation flux, paper presented at Satellite Systems to Measure Radiation Budget Parameters and Climate Change Signal, Int. Radiat. Comm., Igls, Austria, Aug. 29–Sept. 2.

Swinbank, W. C. (1963), Long-wave radiation from clear skies, *Q. J. R. Meteorol. Soc.*, *89*, 339–348.
Tang, B., and Z.-L. Li (2008), Estimating of instantaneous net surface longwave radiation from MODIS cloud-free data, *Remote Sens. Environ.*, *112*, 3482–3492.
Wan, Z. (2008), New refinements and validation of MODIS land-surface temperature/emissivity products, *Remote Sens. Environ.*, *112*(1), 59–74.
Wang, K., and R. E. Dickinson (2013), Global atmospheric downward longwave radiation at the surface from ground-based observations, satellite retrievals, and reanalyses, *Rev. Geophys.*, *51*, 150–185, doi:10.1002/rog.20009.
Wang, T., G. Yan, and L. Chen (2013), Consistent retrieval methods to estimate land surface shortwave and longwave radiative flux components under clear-sky conditions, *Remote Sens. Environ.*, *124*(61-71).
Wang, W., and S. Liang (2009), Estimation of high-spatial resolution clear-sky longwave downward and net radiation over land surfaces from MODIS data, *Remote Sens. Environ.*, *113*(4), 745–754.
Wang, W., and S. Liang (2010), A method for estimating clear-sky instantaneous land-surface longwave radiation with GOES sounder and GORE-R ABI data, *IEEE Geosci. Remote Sens. Lett.*, *7*(3), 708–712.
Wang, W., S. Liang, and T. Meyer (2008), Validating MODIS land surface temperature products using long-term nighttime ground measurements, *Remote Sens. Environ.*, *112*, 623–635.
Wang, W., S. Liang, and J. A. Augustine (2009), Estimating high spatial resolution clear-sky land surface upwelling longwave radiation from MODIS data, *IEEE Trans. Geosci. Remote Sens.*, *47*(5), 1559–1570.
Wild, M., D. Folini, M. Z. Hakuba, C. Schar, S. I. Seneviratne, S. Kato, D. Rutan, C. Ammann, E. F. Wood, and G. Konig-Langlo (2014), The energy balance over land and oceans: An assessment based on direct observation and CMIP5 climate models, *Clim. Dyn.*, doi:10.1007/s00382-00014-02430-z.
Xiong, X., B. N. Wenny, A. S. Wu, W. L. Barnes, and V. V. Salomonson (2009), Aqua MODIS thermal emissive band on-orbit calibration, characterization, and performance, *IEEE Trans. Geosci. Remote Sens.*, *47*(3), 803–814.
Yang, K., J. He, W. Tang, J. Qin, and C. C. K. Cheng (2010), On downward shortwave and longwave radiations over high altitude regions: Observation and modeling in the Tibetan Plateau, *Agric. For. Meteorol.*, *150*, 38–46.
Zhang, X., S. Liang, Z. Song, and H. Niu (2016), Local adaptive calibration of the satellite-derived surface incident shortwave radiation product using smoothing spline, *IEEE Trans. Geosci. Remote Sens.*, *54*(2), 1156–1169.
Zhou, Y., D. P. Kratz, A. C. Wilber, S. K. Gupta, and R. D. Cess (2007), An improved algorithm for retrieving surface downwelling longwave radiation from satellite measurements, *J. Geophys. Res.*, *112*, D15102, doi:10.1029/2006JD008159.